Ferrofluid patterns in Hele-Shaw cells: Exact, stable, stationary shape solutions

Sérgio A. Lira[1,*] and José A. Miranda[2,†]
[1]*Instituto de Física, Universidade Federal de Alagoas, Maceió, Alagoas 57072-900, Brazil*
[2]*Departamento de Física, Universidade Federal de Pernambuco, Recife, Pernambuco 50670-901, Brazil*
(Received 3 December 2015; published 27 January 2016)

We investigate a quasi-two-dimensional system composed of an initially circular ferrofluid droplet surrounded by a nonmagnetic fluid of higher density. These immiscible fluids flow in a rotating Hele-Shaw cell, under the influence of an in-plane radial magnetic field. We focus on the situation in which destabilizing bulk magnetic field effects are balanced by stabilizing centrifugal forces. In this framing, we consider the interplay of capillary and magnetic normal traction effects in determining the fluid-fluid interface morphology. By employing a vortex-sheet formalism, we have been able to find a family of exact stationary N-fold polygonal shape solutions for the interface. A weakly nonlinear theory is then used to verify that such exact interfacial solutions are in fact stable.

DOI: 10.1103/PhysRevE.93.013129

I. INTRODUCTION

The Saffman-Taylor problem in Hele-Shaw cells is a paradigmatic example for studying the development of complex interfacial patterns in confined geometry [1]. It takes place when a fluid displaces a more viscous one in the narrow passage separating two parallel glass plates. The interplay between surface tension and viscous forces makes the two-fluid interface unstable, giving rise to the formation of characteristic fingering structures [2]. Visually striking interfacial patterns can also be produced in a rotating Hele-Shaw setup [3–5], where the cell rotates with constant angular velocity and the density difference between the fluids drives the system unstable.

An alternative way to generate interesting fingered morphologies is to consider the interfacial disturbances generated when a magnetic fluid (e.g., a ferrofluid) droplet is confined in a Hele-Shaw cell and an external magnetic field is applied. Ferrofluids [6–8] are stable colloidal suspensions where nanometer-sized magnetic particles are dispersed in a nonmagnetic carrier fluid. These magnetic fluids present a superparamagnetic behavior and are distinguished by their prompt response to even modest magnetic stimuli. In this case, the competition between surface tension and magnetic forces can create a vast variety of interfacial shapes ranging from labyrinthine structures [9–11] to spiral and protozoanlike patterns [12,13].

No matter what the nature of the driving force (viscous, centrifugal, magnetic, etc.) acting against surface tension is, it is well known that the determination of exact solutions for the finger shapes in Hele-Shaw flows is not a trivial task. Since these exact solutions are not restricted to small perturbations of an initially circular two-fluid interface, they are particularly useful in providing valuable insights into possible complex shapes assumed by the emerging fingering structures at fully nonlinear regimes. However, in contrast to the equivalent zero-surface-tension situation (see, for example, [14–22] and references therein), the establishment of such exact solutions when nonzero capillary forces take effect are relatively scarce.

In the context of viscous fingering, only three general types of systems allow the determination of exact finger shape solutions with finite surface tension, where capillary forces balance the corresponding driving forces of the problem. The first one, which refers to the development of fingers in rectangular (channel) Hele-Shaw cells, was originally examined in Ref. [23] and was later more thoroughly investigated in Ref. [24]. In these works, the resulting exact stationary solutions display teardroplike shapes that resemble the classical Euler elastica solutions of ideal bending rods [25,26]. A second system studies the elasticalike exact stationary solutions that arise in rotating Hele-Shaw cells, when surface tension is matched by centrifugal forces [24,27,28] at the fluid-fluid boundary. In these articles, regular N-fold petal-shaped patterns set in, as well as peculiar cusped structures connected to satellite drops located at infinity. It is worth noting that similar types of steady patterns arise in various other systems including closed elastic wires under pressure in a plane [29,30], cylindrical fluid membranes [31], two-dimensional vesicles [32], and softly constrained films [33]. Still, in the Hele-Shaw cell context, there are unstable N-fold symmetric solutions (which look like polygons with smoothed edges) presented in Ref. [34], where the regularizing action of both surface tension and kinetic undercooling are considered. Families of unstable N-fold solutions similar to the related problem for the porous medium equation were also found in Refs. [35–38].

A third kind of system involves the consideration of magnetic forces acting on magnetic fluids (ferrofluids and magnetorheological fluids [39–41]) subjected to a radial magnetic field in motionless Hele-Shaw cells [42,43] and to an azimuthal magnetic field in both rotating [44] and motionless [45,46] Hele-Shaw cell arrangements. The action of the external magnetic fields induces the appearance of generalized unstable elasticalike stationary solutions, where various types of polygon-shaped structures and starfishlike patterns have been obtained.

Despite the nontrivial nature and the morphological variety exhibited by the stationary shape solutions obtained in Refs. [23,24,27,28,34–38,42–46], in most of these studies it has been found that such solutions are *unstable*. This means that these solutions are possibly very difficult to directly observe in real experimental realizations, so their relevance to the dynamics of such systems is uncertain. Remarkably,

*sergio@fis.ufal.br
†jme@df.ufpe.br

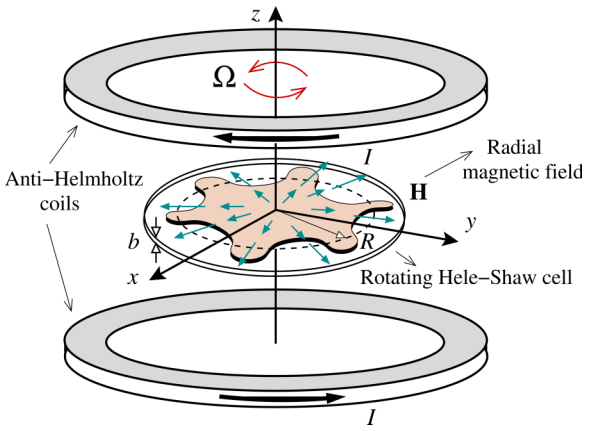

FIG. 1. Representative sketch of a rotating Hele-Shaw cell setup containing a viscous ferrofluid droplet subjected to an applied radial magnetic field **H** produced by anti-Helmholtz coils. The outer fluid is nonmagnetic and has higher density. The cell rotates around the z axis with constant angular velocity Ω. The directions of the electric currents I in both coils are also indicated. In this configuration the magnetic field destabilizes the interface, while surface tension and centrifugal forces stabilize it.

it seems that the only existing case in which linearly stable, nonzero-surface-tension, exact stationary solutions are available is offered by a biology-motivated fluid model, where the morphology and anisotropic growth of polarized tissues is studied [47]. The authors of Ref. [47] have obtained circular and oval-like exact shape solutions in a friction-dominated regime and have checked numerically that these solutions are generically stable to small perturbations. Nevertheless, an investigation about the possibility of obtaining stable exact stationary shape solutions in the physical context of a viscous fluid fingering problem is still lacking.

In this work we consider a physical system in which the combined action of surface tension and centrifugal and magnetic forces result in the uprising of exact *stable* stationary shape solutions for the two-fluid interface. More specifically, we examine the interfacial pattern formation process that occurs in a rotating Hele-Shaw cell containing an initially circular ferrofluid droplet, which is surrounded by a more dense nonmagnetic fluid (see Fig. 1). The cell rotates around the z axis with constant angular velocity Ω. An externally applied radial magnetic field is produced by two Helmholtz coils carrying electric currents that flow in opposite directions. Under such circumstances, the magnetic force tends to destabilize the interface separating the two fluids, while surface tension and centrifugal forces act to stabilize it. The interplay of these competing physical effects will allow the appearance of stable interface shape solutions. It should be emphasized that the special physical system we study in this work, which leads to stable stationary solutions, was not treated in Refs. [4,24,27,28,39–46].

The rest of this paper is outlined as follows. In Sec. II the moving boundary problem is described in detailed. We employ a fully nonlinear vortex-sheet formalism to gain analytical and numerical insight into the establishment of these innovative, stationary ferrofluid patterns. Section III presents the analytical determination of the exact stationary shapes. Linear and weakly nonlinear stability analyses are then utilized in Sec. IV to investigate the stable nature of such magnetic fluid structures. Finally, in Sec. V we present our chief conclusions and final remarks.

II. DESCRIPTION OF THE MOVING BOUNDARY PROBLEM

Figure 1 illustrates an incompressible ferrofluid droplet of unperturbed radius R, viscosity η_1, and density ρ_1 located between two narrowly spaced flat plates of a Hele-Shaw cell of thickness b. The outer, surrounding fluid is nonmagnetic and has viscosity η_2 and density ρ_2. The surface tension at the immiscible fluid-fluid interface is nonzero and denoted by γ. We consider that the ferrofluid droplet is subjected to an applied in-plane radial magnetic field

$$\mathbf{H} = \frac{H_0}{L} r \hat{\mathbf{e}}_r, \tag{1}$$

where r is the radial distance from the origin of the coordinate system located at the center of the droplet, H_0 is a constant, L is a characteristic length, and $\hat{\mathbf{e}}_r$ is a unit vector in the radial direction. It is worth pointing out that this specific magnetic field configuration can be realistically generated by a pair of identical Helmholtz coils whose currents are equal and flow in opposite directions, in an anti-Helmholtz arrangement [43,48]. A magnetic body force $\mathbf{F} \sim \nabla H$, where $H = |\mathbf{H}|$ is the local magnetic field intensity, acts on the magnetic fluid pointing in the outward radial direction [6,45]. Since the applied magnetic field presents a natural nonzero gradient, we take it as the main local field contribution to the magnetic body force, therefore neglecting minor demagnetizing effects. Moreover, the cell is rotated with constant angular velocity Ω about the z axis located at the origin, being perpendicular to the plane of the flow. In contrast to previous works on the rotating Hele-Shaw cell [24,27,28,44], here we consider that $\rho_2 > \rho_1$ such that centrifugal force points radially inward and tends to stabilize the circular droplet, acting in opposition to the magnetic body force.

Following the standard approach in Hele-Shaw problems, one starts by neglecting inertial contributions in the three-dimensional (3D) Navier-Stokes equation and by imposing a no-slip boundary condition at the cell plates. Then, by taking a parabolic velocity profile, an effectively 2D flow is obtained by averaging the 3D Navier-Stokes equation over the cell gap direction. By considering the contribution of centrifugal [3] and magnetic [43] forces, one can write a modified Darcy law for the gap-averaged velocity $\mathbf{v}$ of the confined fluids

$$\mathbf{v}_j = -\frac{b^2}{12\eta_j}\nabla\left[\Pi_j + \frac{\rho_j \Omega^2 r^2}{2}\right], \tag{2}$$

where $j = 1$ ($j = 2$) labels the inner (outer) fluid. The gap-averaged generalized pressure Π is defined as [10]

$$\Pi = \frac{1}{b}\int_{-b/2}^{+b/2} [P - \Psi] dz, \tag{3}$$

where P is the 3D pressure,

$$\Psi = \mu_0 \int_0^H M dH = \frac{\mu_0 \chi H^2}{2} \tag{4}$$

represents a magnetic pressure [6,43], and μ_0 denotes the magnetic permeability of free space. In Eq. (4) we used the linear relationship $\mathbf{M} = \chi \mathbf{H}$, with $M = |\mathbf{M}|$ being the magnetization of the ferrofluid and χ its magnetic susceptibility. For the nonmagnetic fluid $\chi = 0$ and $\Psi = 0$.

Since the velocity field is irrotational in the bulk, it is convenient to state our moving boundary problem in terms of velocity potentials ϕ_j, where $\mathbf{v}_j = -\nabla\phi_j$. From the incompressibility condition $\nabla \cdot \mathbf{v}_j = 0$ it can be seen that the velocity potential is indeed Laplacian for both fluids, so we have that $\nabla^2\phi_j = 0$. Further specification about the velocity potential is provided by the augmented pressure jump boundary condition at the interface

$$p_1 - p_2 = \gamma\kappa - \tfrac{1}{2}\mu_0(\mathbf{M}\cdot\hat{\mathbf{n}})^2, \tag{5}$$

where $p = [\int_{-b/2}^{+b/2} P dz]/b$ is the gap-averaged pressure and $\hat{\mathbf{n}}$ denotes the unit normal vector at the interface. The first term on the right-hand side of Eq. (5) expresses the conventional contribution related to surface tension and interfacial curvature κ. The second term on the right-hand side of (5) is related to the magnetic nature of the problem: It is commonly known as the magnetic normal traction term [6,7,44] and incorporates the influence of the discontinuous normal component of the magnetization at the interface. This particular magnetic contribution plays a central role in determining the shape of the emergent ferrofluid interfacial patterns. It is worthwhile to note that the magnetic normal traction term acts like the anisotropic force term appearing in Eq. (3) of Ref. [47], which is due to the active stresses acting on the edge of a biological tissue sample.

The remaining boundary condition (commonly known as the kinematic boundary condition [2]) connects the velocity of the ferrofluid with the motion of the two-fluid interface itself and expresses the fact that the normal components of the fluids velocities are continuous across the interface $\mathbf{v}_1 \cdot \hat{\mathbf{n}} = \mathbf{v}_2 \cdot \hat{\mathbf{n}}$. Therefore, the definition of the moving boundary problem is specified by the equations

$$\nabla^2\phi_{1,2} = 0, \tag{6}$$

$$\frac{\partial\phi_1}{\partial n} = \frac{\partial\phi_2}{\partial n}, \tag{7}$$

$$\frac{\partial\phi_1}{\partial s} - \frac{\partial\phi_2}{\partial s} = \Gamma, \tag{8}$$

where $\partial/\partial s = \partial_s$ ($\partial/\partial n = \partial_n$) is the derivative along the tangent (normal) direction to the interface. Equation (7) describes the continuity of the normal velocity at the interface and Eq. (8) expresses the tangential velocity jump of magnitude Γ. This jump originates in a nonzero vorticity region restricted to the interface separating the fluids [49,50]. With the help of the generalized Darcy law (2) and the pressure jump (5), an explicit expression for the vortex-sheet strength can be derived in its dimensionless form

$$\Gamma = 2\partial_s\{\kappa - N_B r^2\chi[1 + \chi(\hat{\mathbf{n}}\cdot\hat{\mathbf{r}})^2] + N_\Omega r^2\} - A\left(\frac{\partial\phi_1}{\partial s} + \frac{\partial\phi_2}{\partial s}\right), \tag{9}$$

where lengths and time are rescaled by r_0 and $[12(\eta_1 + \eta_2)r_0^3]/\gamma b^2$, respectively, and r_0 is a typical length being on the order of the unperturbed droplet radius R. The system is characterized by the dimensionless parameters

$$N_B = \frac{\mu_0 H_0^2 r_0^3}{2\gamma L^2}, \quad N_\Omega = \frac{\Delta\rho\Omega^2 r_0^3}{2\gamma},$$

where $\Delta\rho = \rho_2 - \rho_1 > 0$, as well as by the viscous contrast $A = (\eta_1 - \eta_2)/(\eta_1 + \eta_2)$. The parameter N_B represents the magnetic Bond number and measures the ratio of magnetic to capillary forces. On the other hand, the interplay between centrifugal and surface tension effects is described by a rotational Bond number N_Ω.

Now, with the proper moving boundary problem specified, we are able to analyze all the relevant physical effects that determine the interface evolution by taking a closer look at Eq. (9). The first terms at the right-hand side of Eq. (9), which are the tangential derivatives between curly brackets, are the local part of the vortex sheet, while the potential-dependent terms between large parentheses express the nonlocal character of the time-evolving interface. As a matter of fact, the local terms contain the specific physics of our problem: The term proportional to the curvature κ originates from capillary effects; the term $N_B r^2\chi$ accounts for the magnetic body force arising from the natural gradient of the radial magnetic field in the ferrofluid; the contribution of $N_B r^2\chi^2(\hat{\mathbf{n}}\cdot\hat{\mathbf{r}})^2$ comes from the discontinuity of the magnetization at the interface, that is, it represents the magnetic normal traction effect in the pressure jump condition (5); and, finally, we have the term proportional to N_Ω that quantifies the centrifugal force difference between both fluids. We point out that, in the particular setup considered in this paper, the magnetic body force and the centrifugal force terms possess the same spatial dependence, therefore they can be arranged into a common contribution to the vortex sheet, namely, $2\partial_s[(N_\Omega - N_B\chi)r^2]$.

In the following sections we pursue the goal of finding and characterizing stationary stable solutions of our system by focusing on the vortex-sheet local terms in Eq. (9) arising from the pressure jump condition (5). In order to achieve this, in the rest of this work we give special attention to the specific case where the stabilizing effect of the centrifugal forces exactly balances the destabilizing effect of the magnetic body force. This is possible by setting $N_\Omega = \chi N_B$, which in practice means that we carefully tune rotation to cancel out the radial magnetic field body force. By doing so, we consider only the influence of capillary versus the magnetic normal traction effects on the interface shape and dynamics. This is the key feature displayed by the setup explored in this work, in opposition to usual previous viscous fingering models that explore bulk forces contributions [4,27,28,39–46]. This is also what allows our system to display stable stationary shapes, similar to those obtained in the biological system examined in Ref. [47]. It should be noticed that the case in which $N_\Omega \neq \chi N_B$ (which leads to unstable solutions) also has not been treated in the literature.

III. EXACT STATIONARY SHAPE SOLUTIONS

As in Refs. [42–46], we use the vortex-sheet formalism to obtain the exact stationary shapes of our viscous fingering

problem, which consists in a rotating ferrofluid droplet subjected to a radial magnetic field, obeying the special condition $N_\Omega = \chi N_B$. As discussed in detail in Refs. [24,27], this type of elasticalike stationary solution with nonzero surface tension can be found by imposing a condition of zero vorticity ($\Gamma = 0$) plus considering a stationary state ($\partial\phi_{1,2}/\partial s = 0$) in Eq. (9). We emphasize that, in our setup, this is equivalent to imposing a static equilibrium between the capillary and magnetic normal traction forces at the interface between the inner and outer fluids.

Under such circumstances [$\Gamma = 0$ and $\partial\phi_{1,2}/\partial s = 0$ in Eq. (9)], we find that the curvature of the droplet interface satisfies a nonlinear differential equation

$$\partial_s\{\kappa - N_B r^2\chi[1 + \chi(\hat{\mathbf{n}}\cdot\hat{\mathbf{r}})^2] + N_\Omega r^2\} = 0, \tag{10}$$

which can be readily integrated yielding

$$\kappa = \kappa(r, r\sin\psi) = a + c(r\sin\psi)^2, \tag{11}$$

where a is a constant of integration. Notice that Eq. (11) does not depend on the viscosity contrast A. For brevity we define $c = N_B\chi^2$. In Eq. (11) we have used the fact that $\hat{\mathbf{n}}\cdot\hat{\mathbf{e}}_r = \pm\sin\psi$, where ψ is the angle between the radius vector $\hat{\mathbf{e}}_r$ and the tangent vector $\hat{\mathbf{s}}$ at the interface. Note that c is non-negative, so in order to allow nontrivial solutions κ must change its sign along the curve and we require that $a < 0$.

We wish to study the family of planar curves whose curvature has the general form given by Eq. (11). These curves are the exact stationary solutions we are seeking, which equilibrate the competing magnetic and surface tension forces at the interface. In order to find such solutions we begin by expressing the curvature of the interface in terms of polar coordinates r and φ. By choosing r as a parameter, a differential equation for the curvature of the interface can be written as [42]

$$r\varphi'' + \varphi'(2 + r^2\varphi'^2) = \kappa(r, r\sin\psi)(1 + r^2\varphi'^2)^{3/2} \tag{12}$$

for $r > 0$, where the prime indicates differentiation with respect to r. By performing a convenient change of variables $r\varphi' = \tan\psi$, after some simplifications we find that Eq. (12) assumes the simpler form

$$(r\sin\psi)' = r\kappa(r, r\sin\psi). \tag{13}$$

Remarkably, if we set $w = r\sin\psi$ and use Eq. (11), we deduce at once from Eq. (13) the differential equation

$$w' = r(a + cw^2), \tag{14}$$

whose general solution is given by

$$w(r) = \sqrt{\frac{a}{c}}\tan\left[\frac{\sqrt{ac}}{2}r^2 + C\right], \tag{15}$$

where C is an arbitrary constant. By employing this geometric approach, the problem of determining the shape of the interface is solved once we compute

$$\varphi(r) = \varphi_0 + \int_{r_0}^{r}\frac{1}{\tau}\tan\psi(\tau)d\tau, \tag{16}$$

where $\tan\psi = w(r)/\sqrt{r^2 - w^2(r)}$. Moreover, φ_0 and r_0 are initial plot values for the coordinates and they can be set to $\varphi_0 = 0$ and $r_0 = 1$ without loss of generality. Equations (15) and (16) analytically determine the complete set of stationary solutions of our problem, except for the arbitrary integration constants a and C, which are related to the values of κ and ψ at (r_0,φ_0), respectively. Although we have obtained all the possible stationary solutions of our problem analytically [Eqs. (15) and (16)], the closed plane curves that represent relevant stationary shape solutions of our problem can be conveniently plotted by just solving Eq. (11) numerically.

We proceed by imposing a commensurability condition on the stationary solutions through the theorem of turning tangent [33]

$$\int \kappa ds = 2\pi m, \tag{17}$$

where m is an integer, named the rotation index of the curve, which measures how many times the curve turns with respect to a fixed direction. For our physical drops the interface must be a simple closed curve (without self-crossings), thus $m = 1$. In order to find all physical shapes for a given set of physical parameters (χ, N_B, and $N_\Omega = \chi N_B$), we plot several solutions to Eq. (11) by fixing c, choosing the initial plot condition $\psi(r_0 = 1,\varphi_0 = 0) = \pi/2$, and varying the numerical parameter a. Moreover, we introduce the auxiliary commensurability parameter

$$\delta = \int \kappa ds - 2\pi \tag{18}$$

such that when $\delta = 0$ for a given set of parameters, it means that these parameters produce a closed interface.

By following this procedure, in Fig. 2 we plot δ as a function of a for a fixed value of the physical dimensionless parameter $c = 30$. The dots indicate the solutions of Eq. (11) and the lines are simple linear interpolations of neighboring points. We observe that the curve crosses the axis $\delta = 0$ fourteen times, indicating the values of a associated with possible

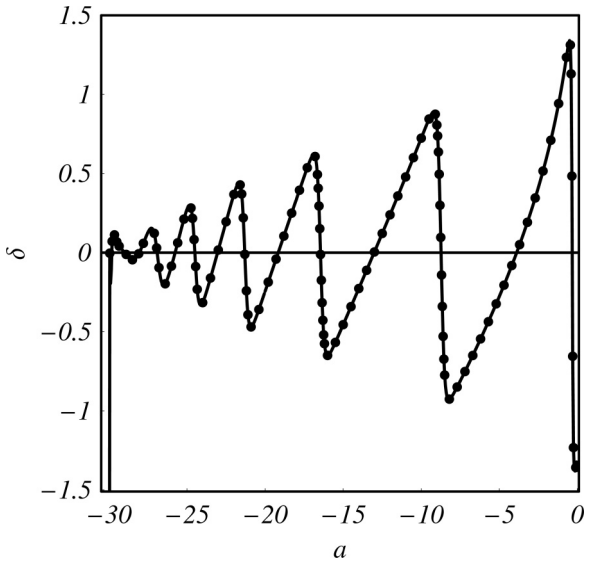

FIG. 2. Plot of the commensurability parameter δ as a function of the integrating constant a for $c = \chi^2 N_B = 30$. The values of a for which $\delta = 0$ (there are 14 of them) determine commensurable stationary shapes.

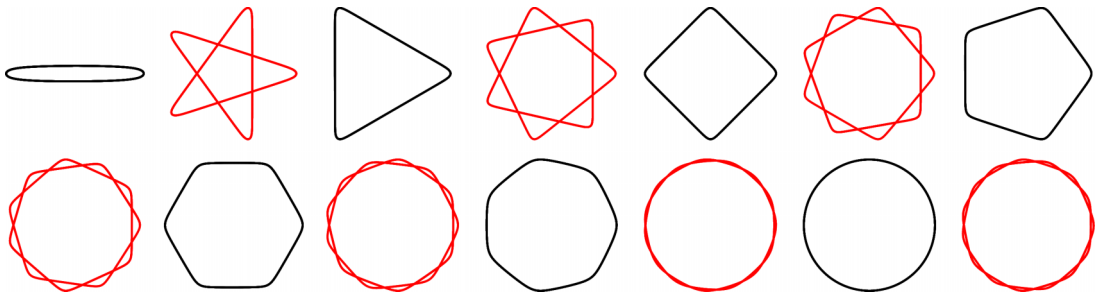

FIG. 3. Commensurable solutions found by using the data presented in Fig. 2. Each shape corresponds to values of a for which $\delta = 0$. From left to right we have $a = -0.3288, -3.8877, -8.7297, -13.0185, -16.4536, -19.1599, -21.3043$ for the top row and $a = -23.0462$, $-24.4995, -25.7647, -26.9147, -28.0621, -28.9931, -29.8200$ for the bottom row.

simple closed curves. Figure 3 illustrates the resulting shapes corresponding to the values of a for which $\delta = 0$. It should be noted that these shapes represent a series of separate stationary patterns and not a time-evolving sequence of events. As one can readily notice by inspecting Fig. 3, there are still some shapes that display interface overlapping (starting to count on the top row, from left to right they correspond to the even numbered structures), which represent nonphysical solutions and therefore should be excluded from our physical analysis. The remaining physical interfacial curves depict polygonlike shapes with sharp tip fingers and fairly straight edges. As the magnitude of a is increased we find that the number of fingers also increases in the structures. In addition, the fingers get smaller in amplitude and become more rounded at the tips, up to the point where the 13th solution is almost circular.

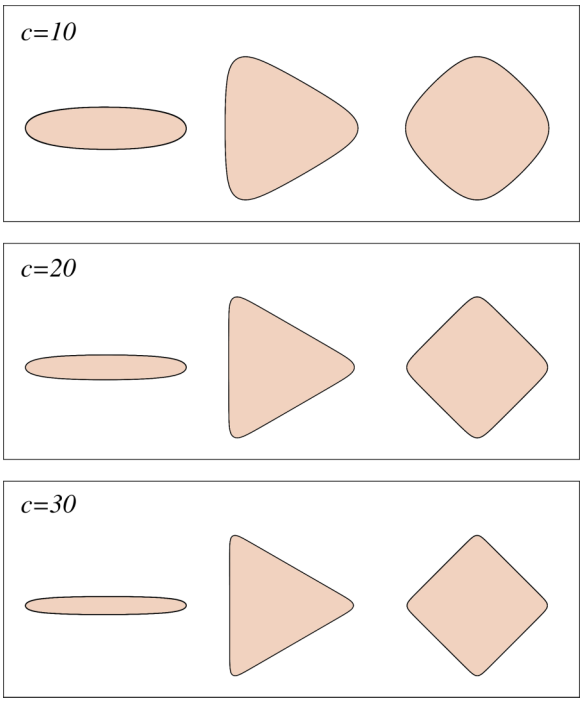

FIG. 4. Typical nonperturbative, stationary shape solutions for a magnetic fluid droplet subjected to rotation and radial magnetic field, considering three values of $c = 10,20,30$. For each value of c the different N-fold patterns ($N = 2,3,4$) are obtained by taking increasingly larger absolute values of the constant of integration a (in a given panel the magnitude of a increases from left to right).

To explore the influence of the parameter c on the morphology of the exact stationary solutions, in Fig. 4 we illustrate the physical N-fold shapes with $N = 2$, 3, and 4, for three different values of $c = 10, 20$, and 30. As explained previously, $c = N_B \chi^2$ quantifies the ratio between the magnetic normal traction contribution and capillary forces and it is related to the tendency of ferrofluid interfacial instabilities to present sharp fingers. As a matter of fact, in Fig. 4 we verify that as c is increased the fingers become increasingly sharper. Although it cannot be seen in this figure, we have also verified that as c increases, the number of stationary solutions also increases.

IV. STABILITY OF THE STEADY SHAPES

In order to analyze the stability of our stationary solutions, we make use of a perturbative mode-coupling approach [44]. In this way, the stationary approximate interface obtained with a weakly nonlinear (WNL) analysis can be compared with the fully nonlinear exact steady shapes, as long as the lengths of the fingers are not too long. We verify that a few perturbative orders can account for the entire exact solution and hence a certain truncation in the number of Fourier modes involved can be regarded as a good representation of the exact shapes. We examine the purely linear (early time) stage of the flow, as well as the weakly nonlinear regime, during which important nonlinear effects (e.g., finger tip sharpening) start to become relevant and stationary amplitudes are achieved.

Within the scope of our second-order mode-coupling theory [51], the perturbed shape of the interface can be written as $\mathcal{R}(\varphi,t) = R + \zeta(\varphi,t)$, where R is the radius of the initially circular two-fluid interface. Here $\zeta(\varphi,t) = \sum_{n=-\infty}^{+\infty} \zeta_n(t) \exp(in\varphi)$ represents the net interface perturbation with complex Fourier amplitudes $\zeta_n(t)$ and discrete azimuthal wave numbers n. We define Fourier expansions for the velocity potential and use the boundary conditions (5) and (7) presented in Sec. II to express ϕ in terms of ζ_n in order to obtain dimensionless mode-coupling differential equations for the system accurate to second order in the perturbation amplitudes. After performing such a weakly nonlinear calculation, the evolution of the perturbation amplitudes is given as

$$\dot{\zeta}_n = \lambda(n)\zeta_n + \sum_{n' \neq 0} [F(n,n')\zeta_{n'}\zeta_{n-n'} + G(n,n')\dot{\zeta}_{n'}\zeta_{n-n'}], \quad (19)$$

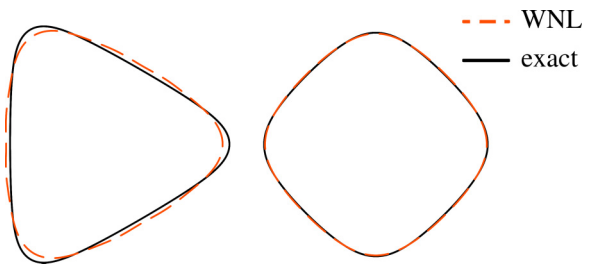

FIG. 5. Comparison between exact (solid curves) and WNL (dashed curves) solutions for the steady interface shape for $c = 10$ and a number of fingers $N = 3,4$.

where the overdot represents a total time derivative with respect to time and

$$\lambda(n) = |n|\left[2N_B\chi^2 - \frac{1}{R^3}(n^2-1)\right] \tag{20}$$

is the linear growth rate. The second-order mode-coupling terms are represented as

$$F(n,n') = \frac{|n|}{R}\left\{N_B\chi^2(1+n'(n-n')) - \frac{1}{R^3}\left[1-\frac{n'}{2}(3n'+n)\right]\right\}, \tag{21}$$

$$G(n,n') = \frac{1}{R}\{A|n|[\mathrm{sgn}(nn')-1]-1\}, \tag{22}$$

where the sgn function equals ± 1 according to the sign of its argument.

By examining Eq. (20) for the linear growth rate, it is evident that the term proportional to χ^2 coming from the normal magnetic traction contribution is destabilizing (induces a positive growth rate). On the other hand, the remaining term is related to capillary forces and tends to stabilize the fluid-fluid interface. The terms appearing in the expression for the function $F(n,n')$ in Eq. (21) arise from the magnetic applied field and surface tension, respectively. In contrast, the function $G(n,n')$ defined in Eq. (22) presents no dependence on magnetic effects. As we will see below, already at second order, by using just a few modes, we are able to obtain stationary solutions of small perturbation amplitudes.

Figure 5 illustrates a comparison between exact stationary shapes and the WNL steady solutions obtained by setting $\dot{\zeta}_n = 0$ for all n in Eq. (19). The solid curves depict the threefold and the fourfold exact stationary patterns presented in the first row of Fig. 4, for which $c = 10$. On the other hand, the dashed curves show the corresponding WNL stationary solutions. Since the exact shapes are not very deformed, the weakly nonlinear approach can be successfully applied to approximate quite well the fully nonlinear results by using only three Fourier modes (namely, $n = N, 2N$, and $3N$, where N is the number of fingers; therefore $N = 3,4$ for threefold and fourfold solutions, respectively).

Now we turn to one last and important aspect related to the stability of the stationary solutions. This is done by setting a system of nonlinear differential equations for only three harmonic modes N, $2N$, and $3N$, by using the mode-coupling equation (19). We proceed by utilizing correspondent cosine perturbation amplitudes a_N, a_{2N}, and a_{3N}, where

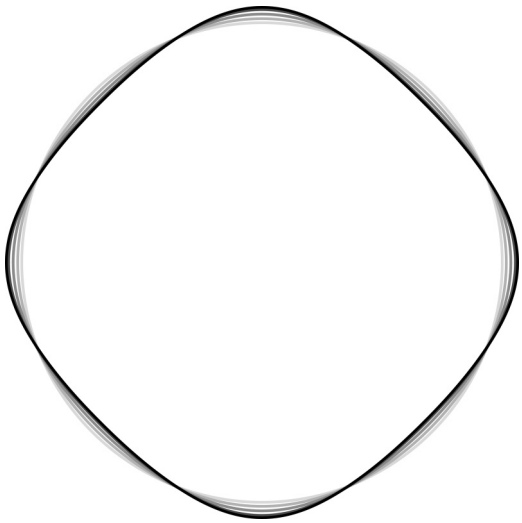

FIG. 6. Time evolution of an initially circular droplet perturbed by a small $n = 4$ Fourier mode, for $c = 10$ and $0 \leqslant t \leqslant 1.35$, in equal time intervals $\Delta t = 0.15$, where darker color curves mean larger values of time. The interface profile for $t > 1.35$ is indistinguishable from the one shown at $t = 1.35$.

$a_n = \zeta_n + \zeta_{-n}$ are real Fourier coefficients. Through a standard linearization process close to the stationary solution, we diagonalize the resulting system of equations, determining the eigenvalues that dictate the stability of the fixed point [44,52]. By doing so, we have verified that the steady solutions shown in Fig. 5 are stable. For these patterns we have three negative eigenvalues, characterizing an attractor point. Additionally, we have found that the unperturbed drop is unstable and therefore if one perturbs an initially circular interface it will evolve towards a nontrivial stationary solution. This situation is illustrated in Fig. 6, which displays the time evolution of a nearly circular droplet perturbed by a fourfold harmonic mode, where $c = 10$. As time advances, the four-fingered perturbation increases and reaches a stationary profile depicted by the shape on the right-hand side of Fig. 5.

Complementary information about the pattern-forming phenomenon depicted in Fig. 6 is provided by Fig. 7, which plots the time evolution of the cosine perturbation amplitudes a_N, a_{2N}, and a_{3N}. We point out that both Figs. 6 and 7 are obtained by numerically solving the following system of nonlinear differential equations derived by considering the coupling of only three cosine modes in Eq. (19):

$$\begin{aligned}\dot{a}_N = {} & \lambda(N)a_N + \tfrac{1}{2}\{[F(N,-N)+F(N,2N)]a_N a_{2N} \\ & + [F(N,-2N)+F(N,3N)]a_{2N}a_{3N} \\ & + G(N,-N)\dot{a}_N a_{2N} + G(N,2N)\dot{a}_{2N}a_N \\ & + G(N,-2N)\dot{a}_{2N}a_{3N} + G(N,3N)\dot{a}_{3N}a_{2N}\}, \end{aligned} \tag{23}$$

$$\begin{aligned}\dot{a}_{2N} = {} & \lambda(2N)a_{2N} + \tfrac{1}{2}\big\{F(2N,N)a_N^2 \\ & + [F(2N,-N)+F(2N,3N)]a_N a_{3N} \\ & + G(2N,N)\dot{a}_N a_N + G(2N,-N)\dot{a}_N a_{3N} \\ & + G(2N,3N)\dot{a}_{3N}a_N\big\}, \end{aligned} \tag{24}$$

$$\begin{aligned}\dot{a}_{3N} = {} & \lambda(3N)a_{3N} + \tfrac{1}{2}\{[F(3N,N)+F(3N,2N)]a_N a_{2N} \\ & + G(3N,N)\dot{a}_N a_{2N} + G(3N,2N)\dot{a}_{2N}a_N\}. \end{aligned} \tag{25}$$

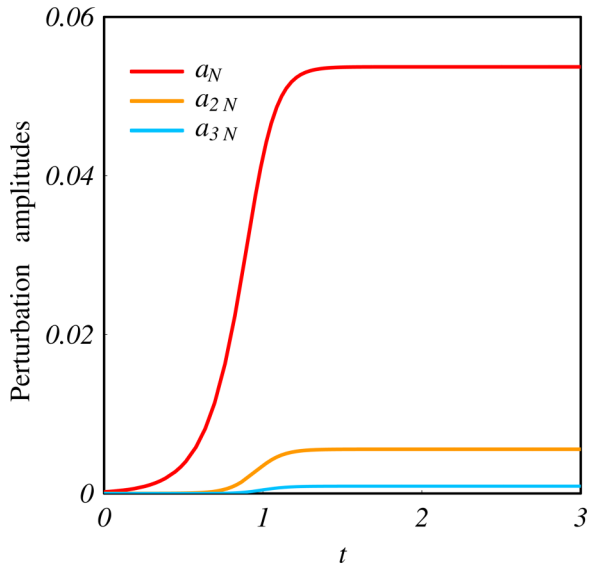

FIG. 7. Time evolution of the cosine perturbation amplitudes $a_N(t)$, $a_{2N}(t)$, and $a_{3N}(t)$, where $N = 4$, for the evolving interface depicted in Fig. 6. It is clear that all amplitudes eventually tend to stationary values.

From Fig. 7 we clearly observe that the weakly nonlinear coupling naturally dictates the enhanced growth of positive harmonic modes, which is the phase that induces finger tip sharpening [51]. It is also evident that after an initial period of growth, all perturbation amplitudes saturate, so they remain unchanged as time progresses. This validates the idea that the system tends to a stationary-state configuration.

V. CONCLUSION

Although exact stationary solutions of the viscous fingering problem are plentiful in the zero-surface-tension limit [14–22], corresponding solutions for the finite-surface-tension case are relatively rare. Recently, the vortex-sheet formalism was successfully used to determine exact stationary shape solutions, when surface tension effects are balanced by either viscous, centrifugal, or magnetic forces [24,27,28,42–46]. However, most of these shape solutions are not stable, indicating that their relevance to actual experimental realizations is unclear. Curiously, as far we can tell, the only stable, exact, stationary shape solutions have been obtained in a biology-motivated system dealing with anisotropic growth of polarized tissues [47].

In this work we have been able to prepare a legitimate viscous fingering, physically motivated setup in which the resulting exact stationary shape solutions are indeed stable. This has been accomplished by considering the situation in which a more dense, ferrofluid droplet is surrounded by a nonmagnetic fluid and subjected to a radial magnetic applied field. The whole fluid dynamic system is confined in the narrow passage that separates two parallel glass plates of a rotating Hele-Shaw cell. In this framework, we employed the vortex-sheet formalism and focused on the situation in which destabilizing magnetic forces are counterbalanced by stabilizing centrifugal effects in the bulk. By doing this, the net effect on the ferrofluid droplet boundary results just from the interplay between capillary and magnetic normal traction contributions. This is our physical analog of the biology-motivated system studied in Ref. [47]. The emergent stationary shape solutions we found define N-fold polygonal-like structures presenting increasingly sharper tips and straighter edges as magnetic effects are intensified. Finally, a weakly nonlinear mode-coupling theory was utilized to verify that such exact stationary shape solutions are actually stable.

In closing, we point out that the vortex-sheet technique we presented in this work arises as a useful alternative to traditional variational methods utilized to determine the stationary shape solutions for flexible, inextensible pressurized wires in a plane (elasticalike problems) [29,30], cylindrical fluid membranes [31], two-dimensional vesicles [32], and softly constrained films [33].

ACKNOWLEDGMENT

J.A.M. thanks CNPq for financial support.

[1] P. G. Saffman and G. I. Taylor, Proc. R. Soc. London Ser. A **245**, 312 (1958).
[2] For review articles see, for instance, D. Bensimon, L. P. Kadanoff, S. Liang, B. I. Shraiman, and C. Tang, Rev. Mod. Phys. **58**, 977 (1986); G. M. Homsy, Annu. Rev. Fluid Mech. **19**, 271 (1987); K. V. McCloud and J. V. Maher, Phys. Rep. **260**, 139 (1995); see also J. Casademunt, Chaos **14**, 809 (2004).
[3] L. Carrillo, F. X. Magdaleno, J. Casademunt, and J. Ortín, Phys. Rev. E **54**, 6260 (1996).
[4] E. Alvarez-Lacalle, J. Ortín, and J. Casademunt, Phys. Fluids **16**, 908 (2004).
[5] J. Casademunt, Eur. Phys. J. Plus **126**, 94 (2011).
[6] R. E. Rosensweig, *Ferrohydrodynamics* (Cambridge University Press, Cambridge, 1985).
[7] E. Blums, A. Cebers, and M. M. Maiorov, *Magnetic Fluids* (de Gruyter, New York, 1997).
[8] D. Andelman and R. E. Rosensweig, J. Phys. Chem. B **113**, 3785 (2009).
[9] A. O. Tsebers and M. M. Maiorov, Magnetohydrodynamics **16**, 21 (1980).
[10] D. P. Jackson, R. E. Goldstein, and A. O. Cebers, Phys. Rev. E **50**, 298 (1994).
[11] J. Kent-Dobias and A. J. Bernoff, Phys. Rev. E **91**, 032919 (2015).
[12] S. Rhodes, J. Perez, S. Elborai, S.-H. Lee, and M. Zahn, J. Magn. Magn. Mater. **289**, 353 (2005).
[13] S. Elborai, D.-K. Kim, X. He, S.-H. Lee, S. Rhodes, and M. Zahn, J. Appl. Phys. **97**, 10Q303 (2005).
[14] S. K. Sarkar, Phys. Rev. A **31**, 3468 (1985).
[15] S. D. Howison, J. Fluid Mech. **167**, 439 (1986).
[16] S. P. Dawson and M. Mineev-Weinstein, Phys. Rev. E **57**, 3063 (1998).

[17] W. S. Dai, L. P. Kadanoff, and S. M. Zhou, Phys. Rev. A **43**, 6672 (1991).
[18] M. Siegel and S. Tanveer, Phys. Rev. Lett. **76**, 419 (1996).
[19] F. X. Magdaleno and J. Casademunt, Phys. Rev. E **57**, R3707 (1998).
[20] J. Casademunt and F. X. Magdaleno, Phys. Rep. **337**, 1 (2000).
[21] V. M. Entov, P. I. Etingof, and D. Y. Kleinbock, Eur. J. Appl. Math. **6**, 399 (1995).
[22] D. Crowdy, Q. Appl. Math. **60**, 11 (2002).
[23] J. F. Nye, H. W. Lean, and A. N. Wright, Eur. J. Phys. **5**, 73 (1984).
[24] E. Alvarez-Lacalle, J. Ortín, and J. Casademunt, Phys. Rev. Lett. **92**, 054501 (2004).
[25] For a historical perspective see C. G. Fraser, Centaurus **34**, 211 (1991).
[26] G. M. Scarpello and D. Ritelli, Meccanica **41**, 519 (2006).
[27] E. S. G. Leandro, R. M. Oliveira, and J. A. Miranda, Physica D **237**, 652 (2008).
[28] R. Folch, E. Alvarez-Lacalle, J. Ortín, and J. Casademunt, Phys. Rev. E **80**, 056305 (2009).
[29] G. Arreaga, R. Capovilla, C. Chryssomalakos, and J. Guven, Phys. Rev. E **65**, 031801 (2002).
[30] P. A. Djondjorov, V. M. Vassilev, and I. M. Mladenov, Int. J. Mech. Sci. **53**, 355 (2011).
[31] V. M. Vassilev, P. A. Djondjorov, and I. M. Mladenov, J. Phys. A: Math. Theor. **41**, 435201 (2008).
[32] S. K. Veerapaneni, R. Raj, G. Biros, and P. K. Purohit, Int. J. Nonlinear Mech. **44**, 257 (2009).
[33] L. Giomi, Soft Matter **9**, 8121 (2013).
[34] M. C. Dallaston and S. W. McCue, Nonlinearity **26**, 1639 (2013).
[35] S. B. Angenent and D. G. Aronson, J. Am. Math. Soc. **14**, 737 (2001).
[36] S. B. Angenent, D. G. Aronson, S. I. Betelú, and J. S. Lowengrub, Physica D **151**, 228 (2001).
[37] D. G. Aronson, J. B. Van den Berg, and J. Hulshof, Eur. J. Appl. Math. **14**, 485 (2003).
[38] S. I. Betelú, D. G. Aronson, and S. B. Angenent, Physica D **138**, 344 (2000).
[39] J. M. Ginder, MRS Bull. **23**, 26 (1998).
[40] G. Bossis, S. Lacis, A. Meunier, and O. Volkova, J. Magn. Magn. Mater. **252**, 224 (2002).
[41] S. Genç and P. P. Phulé, Smart Mater. Struct. **11**, 140 (2002).
[42] R. M. Oliveira, J. A. Miranda, and E. S. G. Leandro, Phys. Rev. E **77**, 016304 (2008).
[43] S. A. Lira, J. A. Miranda, and R. M. Oliveira, Phys. Rev. E **81**, 046303 (2010).
[44] S. A. Lira, J. A. Miranda, and R. M. Oliveira, Phys. Rev. E **82**, 036318 (2010).
[45] E. O. Dias and J. A. Miranda, Phys. Rev. E **91**, 023020 (2015).
[46] E. O. Dias, S. A. Lira, and J. A. Miranda, Phys. Rev. E **92**, 023003 (2015).
[47] C. Blanch-Mercader, J. Casademunt, and J. F. Joanny, Eur. Phys. J. E **37**, 41 (2014).
[48] C.-Y. Chen, Y.-S. Yang, and J. A. Miranda, Phys. Rev. E **80**, 016314 (2009).
[49] G. Tryggvason and H. Aref, J. Fluid Mech. **136**, 1 (1983).
[50] G. Birkhoff, Los Alamos Scientific Laboratory Technical Report No. LA-1862, 1954 (unpublished).
[51] J. A. Miranda and M. Widom, Physica D **120**, 315 (1998).
[52] S. A. Lira and J. A. Miranda, Phys. Rev. E **84**, 016303 (2011).